Journal of Applied Mechanics and Technical Physics, Vol. 35, No. 6, 1994

MODEL OF TURBULENT VISCOSITY FOR COMPUTATION OF THREE-DIMENSIONAL TURBULENT BOUNDARY LAYERS

S. I. Shpak

UDC 532.526.4:532.526.3

Among the large number of methods for computation of turbulent boundary layers (e.g., [1-6]) the turbulent viscosity model for computation of two-dimensional turbulent boundary layers stands out because it has been tested on a large body of experimental data. Most of those experiments were chosen by the Stanford conference [8] as control experiments for comparing numerical computations of turbulent boundary layers. Test computations in [7] were carried out for flows over a wide range of positive and negative pressure gradients, permeability parameters (injection and suction), roughness, heat exchange, and Mach and Reynolds numbers, including the laminar–turbulent transition zone. Moreover, this model has been used very extensively in computations of detached flows in angular configurations within the framework of the viscid–inviscid interaction problem [9]. All of this leads to the conclusion that this model of turbulent viscosity is one of the best in the class of algebraic models for computations of two-dimensional flows. Three-dimensional turbulent boundary layers are the object of many experimental and computational–theoretical studies. Analysis of such flows was the subject of, e.g., a symposium in West Berlin in 1982 [5]. The symposium focused particular attention on economical methods of computing the characteristics of three-dimensional boundary layers, which are used successfully in practice. It was noted that only limited experimental information is suitable for testing numerical computations of three-dimensional turbulent flows. Computation of three-dimensional flows requires the maximum possible computer resources and it is not always justifiable to make the problem more complicated by using differential models of turbulence. In this study we have verified the applicability of the algebraic model of turbulent viscosity [7] under the conditions of three-dimensional boundary layers.

The system of equations of a three-dimensional turbulent boundary layer in an orthogonal coordinate system has the form

$$\rho u\frac{\partial u}{\partial x}+\rho v\frac{\partial u}{\partial y}+\rho w\frac{\partial u}{\partial z}-j\frac{\rho w^2}{x}=-\frac{\partial p}{\partial x}+\frac{\partial \tau_{xy}}{\partial y}; \tag{1}$$

$$\frac{\partial p}{\partial y}=0; \tag{2}$$

$$\rho u\frac{\partial w}{\partial x}+\rho v\frac{\partial w}{\partial y}+\rho w\frac{\partial w}{\partial z}+j\frac{\rho uw}{x}=-\frac{\partial p}{\partial z}+\frac{\partial \tau_{yz}}{\partial y}; \tag{3}$$

$$\frac{1}{x^j}\frac{\partial ux^j}{\partial x}+\frac{\partial v}{\partial y}+\frac{\partial w}{\partial z}=0, \tag{4}$$

where u, v, and w are the components of the velocity vector; ρ is the density; p is the pressure; j = 0, x, y, z are the Cartesian coordinates and j = 1, $\partial z = x\partial\vartheta$, x, ϑ are the polar coordinates (x, y, ϑ); and τ_{xy} and τ_{yz} are the components of the tensor of tangential stresses, which are dominant in the boundary-layer approximation:

$$\tau_{xy}=\mu\frac{\partial u}{\partial y}-\overline{\rho u'v'},\ \tau_{yz}=\mu\frac{\partial w}{\partial y}-\overline{\rho w'v'}. \tag{5}$$

Here μ is the dynamic viscosity; u', v', and w' are the pulsating components of the velocity in turbulent flow; and an overbar denotes averaging over time. The coordinate system is chosen so that the x axis coincides with the direction of the mainstream,

Novosibirsk. Translated from Prikladnaya Mekhanika i Tekhnicheskaya Fizika, No. 6, pp. 92-99, November-December, 1994. Original article submitted December 9, 1993; revised version submitted January 14, 1994.

0021-8944/94/3506-0898$12.50

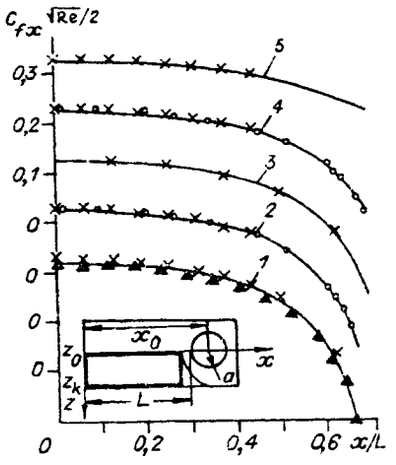

Fig. 1

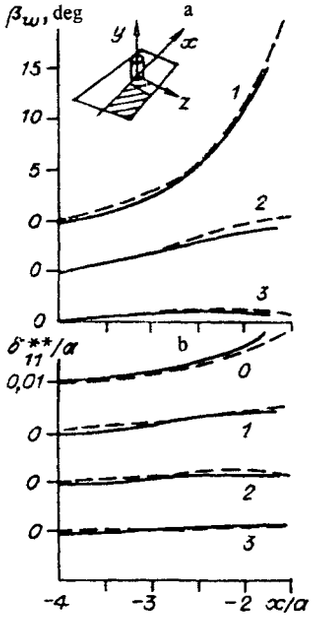

Fig. 2

the z axis lies on the surface of the body, and the y axis is perpendicular to the surface. The solution is sought in the region Ω ($x_0 \leq x \leq x_L$, $z_0 \leq z \leq z_k$, $0 \leq y \leq Y$). The boundary conditions for the system (1)-(4) are the usual ones for a boundary-layer problem: no slip on the surface of the body ($u = 0$, $v = 0$, and $w = 0$ for $y = 0$), distribution of the parameters of viscous flow on the outside boundary of the boundary layer [either the velocity distributions $u = u(x, z)$, $w = w(x, z)$ or the pressure-coefficient distributions $C_p(x, z) = (p(x, z) - p_\infty)/(0.5\rho_\infty U_\infty^2)$ are given, and the angles α of deviation of the streamlines of the external flow from the direction of the mainstream for $y = Y$]. The boundary conditions for the boundary-layer equations are not given in the planes $z_k = \text{const}$ and $x_L = \text{const}$. In this study we considered only flows that have either a plane of flow or a symmetry plane ($z_0 = \text{const}$). The flow parameters on such planes can be found by solving the quasi-two-dimensional boundary-layer problem and can then be used to specify the initial data. If we differentiate Eq. (3) with respect to z and take $w_z = \partial w/\partial z$ to be a new independent variable (also noting that $w \equiv 0$), we obtain a system of equations [instead of (1)-(4)] for the symmetry plane or plane of flow:

$$\rho u \frac{\partial u}{\partial x} + \rho v \frac{\partial u}{\partial y} = -\frac{\partial p}{\partial x} + \frac{\partial \tau_{xy}}{\partial y}; \tag{6}$$

$$\rho u\frac{\partial w_z}{\partial x}+\rho v\frac{\partial w_z}{\partial y}+\rho w_z^2+j\frac{\rho u w_z}{x}=-\frac{\partial^2 p}{\partial z^2}+\frac{\partial}{\partial y}\left(\frac{\partial \tau_{yz}}{\partial z}\right); \tag{7}$$

$$\frac{1}{x^j}\frac{\partial u x^j}{\partial x}+\frac{\partial v}{\partial y}+w_z=0. \tag{8}$$

In the plane x_0 = constant given are either the experimental velocity profiles or the power-law profiles of the projection of the velocity vector onto the direction of the streamline of the external flow $u_0/u_{0e} = (y/Y)^{1/n}$ (the index e denotes that the quantity belongs to the outside boundary of the boundary layer and the index 0 denotes initial data). The exponent n is calculated, in accordance with [10], from $n = 2/(H-1)$, where H is the boundary-layer form parameter. The profile that is normal to the streamline of the external flow of the velocity component w_0 is given on the assumption that the profiles have a delta configuration in the plane of the hodograph (u_0, w_0) [11]:

$$\frac{w_0}{u_{0e}}=\frac{u_0}{u_{0e}}\operatorname{tg}\beta_0 \text{ for } \frac{u_0}{u_{0e}}<\frac{2\alpha_0}{\operatorname{tg}\beta_0+2\alpha_0}, \text{ and}$$

$$\frac{w_0}{u_{0e}}=2\alpha_0\left(1-\frac{u_0}{u_{0e}}\right) \text{ in the remaining profiles.}$$

The profiles u_0 and w_0 are then converted to the profiles u and w by means of the formulas $v_0=\sqrt{u_0^2+w_0^2}$, $\alpha=\alpha_0+\operatorname{arctg}(w_0/u_0)$, $u/u_e=(v_0/v_{0e})\cos\alpha$, and $w/u_e=(v_0/v_{0e})\sin\alpha$. With u and w known, the profiles of the third component v were obtained from the numerical solution of the equation derived from Eqs. (1) and (4) by eliminating the derivative $\partial u/\partial x$ from them:

$$v\frac{\partial u}{\partial y}-u\frac{\partial v}{\partial y}+w\frac{\partial u}{\partial z}-u\frac{\partial w}{\partial z}=-\frac{1}{\rho}\frac{\partial p}{\partial z}+\frac{1}{\rho}\frac{\partial}{\partial y}\mu\frac{\partial u}{\partial y}.$$

To describe the two components of the Reynolds stress tensor which appear in (5), we introduce their relation to the field of mean velocities in the form proposed by Boussinesq [10]:

$$-\overline{\rho u'v'}=\mu_{tx}\partial u/\partial y,\ -\overline{\rho w'v'}=\mu_{tz}\partial w/\partial y.$$

The turbulent viscosity is also assumed to be locally isotropic, i.e., $\mu_t=\mu_{tx}=\mu_{tz}$. The turbulent viscosity μ_t has the form

$$\mu_t=\rho l^2\sqrt{\left(\frac{\partial u}{\partial y}\right)^2+\left(\frac{\partial w}{\partial y}\right)^2}. \tag{9}$$

The quantity l in (9) is determined, in accordance with [7], from

$$l=\begin{cases} ky\left[1-\exp\left(-\dfrac{y\sqrt{\tau\rho}}{\mu A}\right)+\exp\left(-\dfrac{y\sqrt{\tau/\tau_w}A_\tau}{Ah}\right)\right] & \text{for } y\leqslant\dfrac{\lambda\delta}{k}, \\ \lambda\delta & \text{for } y>\dfrac{\lambda\delta}{k}. \end{cases} \tag{10}$$

In (10) h is the height of a roughness irregularity; A_τ is a constant that depends on the type of roughness; $k = 0.4$ is the Karman constant; $\tau=\sqrt{\tau_{xy}^2+\tau_{yz}^2}$; in the region $y \leq \lambda\delta/k$ we calculate τ_{xy} and τ_{yz} as

$$\tau_{xy}=(\tau_{xy})_w+y\frac{\partial p}{\partial x}+\rho\left(v\frac{\partial u}{\partial y}\right)_w y,\ \tau_{yz}=(\tau_{yz})_w+y\frac{\partial p}{\partial z}+\rho\left(v\frac{\partial w}{\partial y}\right)_w y.$$

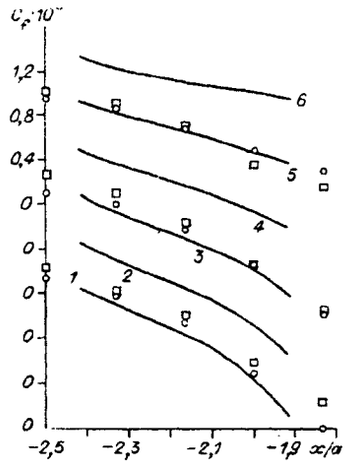

Fig. 3

Here the index w denotes parameters on the surface of the body. These expressions are obtained by expanding $\tau_{xy} + \tau_{yz}$ in a Taylor series near the surface of the body and substituting the results into Eqs. (1) and (3), respectively. A set of correction functions for λ and A is proposed in [7]. In the case of incompressible flows the assumption is that A = 26, and

$$\lambda = \lambda_0/(1 + \tanh F),$$

where $\lambda_0 = 0.09$; $F = \sqrt{3.6\cdot 10^{-5}\mathrm{Re}_1}|\nabla\varphi|\delta_1^*$; and $\varphi = (\delta_1^*/\tau_w)|\nabla P|$ is the Clauser equilibrium principle; $\mathrm{Re}_1 = (u_\infty \rho_\infty \delta_1^*)/\mu_\infty$; and $|\nabla\varphi| = \sqrt{(\partial\varphi/\partial x)^2 + (\partial\varphi/\partial z)^2}$. For computation of laminar and transition boundary layers an intermittence coefficient γ is introduced in much the same way as in [7]:

$$\gamma = 1 - \exp\left[-5.95\left(\frac{x - x_b}{x_e - x_b}\right)^2\right]$$

(x_b, x_e are the coordinates of the beginning and end of the zone of the laminar–turbulent transition zone). The "overall" viscosity coefficient, therefore, is $\mu_\Sigma = \mu + \gamma\mu_t$, and Eqs. (5) have the form

$$\tau_{xy} = \mu_\Sigma \frac{\partial u}{\partial y}, \quad \tau_{yz} = \mu_\Sigma \frac{\partial w}{\partial y}.$$

The quantity δ^{*1}, which enters into the correction functions, is the displacement thickness of the three-dimensional boundary layer; it has the same physical meaning as in the case of plane flow and is calculated from the equation [12]

$$\frac{\partial}{\partial x}(u_e\delta_1^* - v_e\delta_{11}^*) + \frac{\partial}{\partial z}(w_e\delta_1^* - v_e\delta_{12}^*) = 0. \tag{11}$$

Here $v_e = \sqrt{u_e^2 + w_e^2}$, a $\delta_{11}^* = \int_0^\delta (u_e - u)/v_e dy$ и $\delta_{12}^* = \int_0^\delta (w_e - w)/v_e dy$ pertain to v_e and not to u_e and w_e. This substitution prevents divergence of the integrals as $w \to 0$. In a three-dimensional flow the integrals δ_{11}^* δ_{12}^* are physically meaningless and are not components of the displacement thickness. On the flow surface Eq. (11) becomes

$$\frac{\partial}{\partial x}[u_e(\delta_1^* - \delta_{11}^*)] + \delta_1^*(w_z)_e - v_e(\delta_{12}^*)_z = 0, \tag{12}$$

where $(\delta_{12}^*)_z = \int_0^\delta \frac{(w_z)_e - w_z}{u_e} dy$.

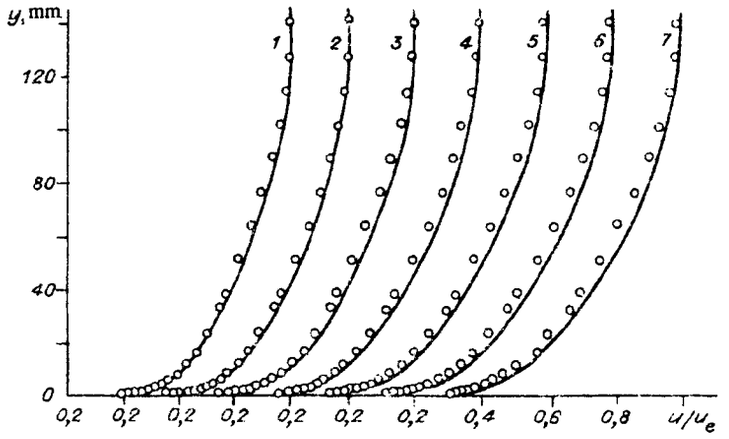

Fig. 4

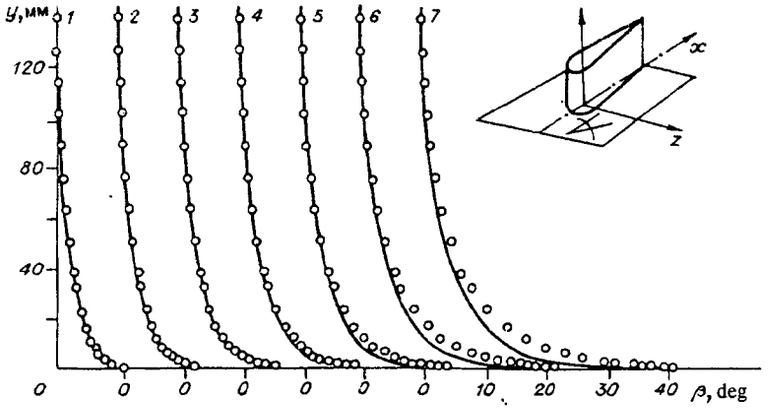

Fig. 5

The differential equations (1)-(4), (6)-(8), (11), and (12) are replaced by finite-difference analogs, using an implicit scheme of the second order of approximation in the coordinates y and z and the first order in the coordinate x. The resulting systems of algebraic equations were solved by marching technique for coordinates x and z and vector tridiagonal inversion for the y coordinate. The computational grid is chosen to match the conditions of the specific problem, with a rigid mesh size in the x and z directions and adjustment of the mesh size in the y direction as the boundary layer grows. The grid spacing is assumed to be uneven along all three coordinates. The given algorithm was the basis for a computing program for the BÉSM-6 computer, which was used for all the computations made here.

RESULTS OF COMPUTATIONS

Computations were carried out for two configurations: a boundary layer on a plate with an obstacle in the form of a vertical cylinder or profile in the flow on the lee side of a delta half-wing, set at the angle of attack. Experimental data, obtained in [11, 13], as well as calculations [14], performed using the differential $k-\varepsilon$ model of turbulence, are available for such flows. Such flows were chosen because of the recommendation of the EUROMECH 60 conference [8] that they be used as control problems for comparing different methods of calculating three-dimensional boundary layers, since in those problems the characteristics of the flow depend on all three coordinates.

Plate with Cylinder. The method of computation and the algorithms of the program we first calculated a laminar boundary layer on a plate with an obstacle in the form of a vertical round infinite cylinder. The outside flow for such a problem is determined from the formula [15]

$$u_e = 1 - \frac{(\Delta z)^2 - (\Delta x)^2}{[(\Delta x)^2 + (\Delta z)^2]^2}, \quad w_e = -2\frac{\Delta z \Delta x}{[(\Delta x)^2 + (\Delta z)^2]^2}.$$

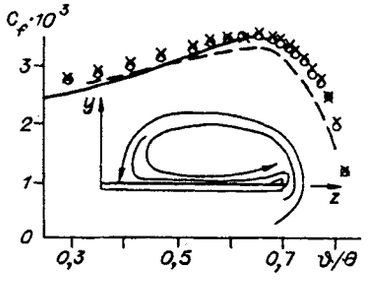

Fig. 6

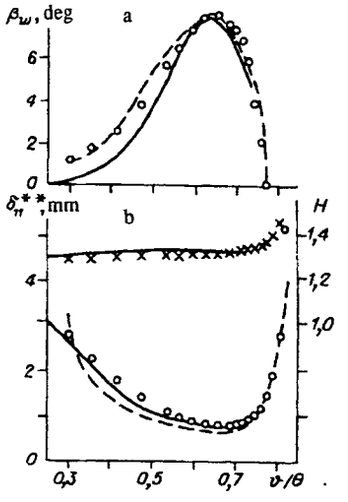

Fig. 7

Here $\Delta z = (z - z_0)/a$; and $\Delta x = (x - x_0)/a$. The range of the calculation and the initial data was chosen as follows: $x_0/a = 7.492$, a = 061 m, $u_\infty = 30.5$ m/sec, L = 3.2192 m, $z_k/a = 1.4$ (the index ∞ denotes mainstream parameters). Figure 1 shows the calculated values of the local friction coefficient for five cross-sections ($z/a = 0$, 0.5, 0.8, 1.0, and 1.4 – lines 1-5, respectively; the crosses represent the data of [15], circles represent the data of [16], and triangles represent the data of [17]). A comparison of the calculated results with the results of other studies enables us to conclude that algorithms and programs function properly and we can proceed to verify the applicability of the given relations to turbulent viscosity.

A turbulent boundary layer for the same problems was calculated for the initial data, as in [14]: $Re_{\delta_{11}}^{**} = U_\infty \delta_{11}^{**} \rho_\infty / \mu_\infty = 50{,}000$, $x/a = -4$, $\delta_{11}^{**} = 0.11a$, H = 1.26, and $z_k/a = 3$. Figure 2 shows the values of the angle of the limiting streamlines (a) and the x component of the momentum thickness δ_{11}^{**} (b) (the dashed lines represent the data of [14]). Some differences from computations using more complicated models for turbulent viscosity (the $k-\varepsilon$ model was used in [14]) manifest themselves in the earlier position of the break line (at a distance $x/a = -1.7$ from the axis of the cylinder) than in [14] (at $x/a = -1.54$). Otherwise the agreement is entirely satisfactory.

Plate with Profile. Computations were performed for a turbulent boundary layer on a plate with an obstacle in the form of a symmetric infinite profile [11], whose front section was formed by a round cylinder with radius $a = 0.3048$ m. The computation was started from a distance $x/a = -2.5$ from the axis of the cylinder and was continued up to the break line. The mainstream velocity $u_\infty = 60.96$ m/sec. Smoothed experimental velocity profiles were chosen as the initial profiles. The parameters of the outside flow were calculated from the measured distribution of the pressure coefficient $C_p = (p - p_\infty)/(0.5 \rho_\infty U_\infty^2)$ and the angles α of the deviation of the streamline of the outside flow from the direction of the mainstream. Figure 3 shows the distribution of the friction coefficient C_f for six cross sections ($z/a = 0$, 0.0833, 0.1667, 0.25, 0.3333, and 0.4167 – lines 1-6, respectively; the symbols represent the experiments of [11]). Figures 4 and 5 show the profiles of the longitudinal

velocity component u/u_e and the angle of deviation β of the local streamlines in the thickness of the boundary layer from the direction of the streamlines of the outside flow for one cross section $z/a = 0.4167$ (solid line – calculation; symbols – experiment; profiles 1-7 correspond to the sections for the coordinate x/a, measured from the axis of the cylinder: -2.42, -2.33, -2.25, -2.17, -2.08, -2.03, and -1.93). The comparison of the calculated results with the experimental data is satisfactory on the whole. The calculated value of the turn of the flow inside the boundary layer is observed to lag somewhat (by roughly 12%) behind the turn found experimentally as the break line is approached. This may be the case because the direction of the mainstream and the axis of the model in the experiment were misaligned (by about 1.16 cm) and as a result the transverse pressure gradient of the outside flow in the calculation was too low in comparison with the actual conditions of the experiment.

Delta Wing. In this example we calculate a turbulent boundary layer induced by a vortex, which comes off the windward side of a delta half-wing, set at an 8° angle of attack (Fig. 6). The vortex then attaches itself to the lee side near the root chord and breaks away for a second time near the wing edge. The region of computation lies between the line of vortex attachment on the lee side and its break line. This flow was studied experimentally in [13] and computed in [14], using the $k-\varepsilon$ turbulence model. The computation was carried out in a polar coordinate system in the region $r = 2.53$-5.53 m and $\vartheta/\theta = 0.25$-0.29 for a mainstream velocity $U_\infty = 60$ m/sec. In contrast to [14], the condition for conical flow ($\partial u_e/\partial x = 0$, $\partial p/\partial x = 0$, $\partial w_e/\partial x = 0$) was not used in the computation since it was not consistent with the experimental data (the values of the pressure coefficient C_p measured in [13] were not constant along the wing). In our computation, therefore, we used the C_p distribution measured experimentally for the given outside flow. Figure 6 illustrates the structure of the flow and the calculated friction coefficients (solid curve) and shows the calculated [14] (dash-dot line) and experimental [13] (symbols) results. Figure 7a shows the angles of deviation β_w of the streamlines near the wall and Fig. 7b shows the values of the momentum thickness δ_{11}^{**} (circles) and the boundary-layer form parameter H (crosses). A comparison was made only for one section, in which the measurements were made in the experiment. The values of the dimensionless polar angle ϑ/θ ($\theta = 14°$) are measured along the horizontal axis. As follows from Figs. 6 and 7, the results of calculations of the integrated boundary-layer characteristics agree satisfactorily with the experimental data and the calculations [14].

In summary, the results of our computations make it possible to conclude that the proposed model of turbulent viscosity is suitable for computation of three-dimensional incompressible boundary layers. In [7] this model was used for calculations of compressed flows and in [9], for calculations of two-dimensional detached flows on the basis of the boundary-layer theory. Since this model has been demonstrated to be applicable for a wide range of conditions, it is desirable to check the possibility of also using it for computations of ultrasonic detached flows on the basis of averaged Navier–Stokes equations.

REFERENCES

1. W. C. Reynolds, "Advances in the computation of turbulent flows," Adv. Chem. Eng., **9** (1974).
2. T. L. Chambers and D. S. Wilcox, "Critical study of two-parameter models for closing a system of equations of a turbulent boundary layer," RTK, **15**, No. 6 (1977).
3. K. K. Fedyaevskii, A. S. Ginevskii, and A. V. Kolesnikov, Computation of a Turbulent Boundary Layer of an Incompressible Liquid [in Russian], Sudostroenie, Leningrad (1973).
4. Turbulent Flows in a Boundary Layer. Part 2. Computational and Experimental Studies [in Russian], TsAGI (N. E. Zhukovskii Central Aerohydrodynamic Institute), Moscow (1980), No. 575.
5. Three-Dimensional Turbulent Boundary Layers [Russian translation], Mir, Moscow (1985).
6. W. F. Klinksiek and F. J. Pierce, "A finite difference solution of the two- and three-dimensional incompressible turbulent boundary layer equations," Trans. ASME Ser. I, J. Fluids Eng., **95**, No. 3, 445 (1973).
7. V. N. Dolgov, V. M. Shulemovich, and S. I. Shpak, "Turbulent viscosity for computation of two-dimensional boundary layers over a wide range of pressure gradients, Mach and Reynolds numbers, and permeability parameters" [in Russian], Preprint ITPM No. 17 (Institute of Theoretical and Applied Mechanics), Akad. Nauk SSSR, Otd. Sib., Novosibirsk (1978).
8. Computation of Turbulent Boundary Layers, Proceedings of AFOSR–IFP–Stanford Conference, Stanford, Calif. (1969).

9. L. V. Golish and V. N. Dolgov, "Using the properties of self-similarity of flow in the zone of return currents for simulation of detached flows," Simulation in Mechanics [in Russian], VTs ITPM (Computing Center, Institute of Theoretical and Applied Mechanics) Akad. Nauk SSSR, Otd. Sib., Novosibirsk (1988).
10. G. Schlichting, Boundary Layer Theory, McGraw-Hill, New York (1968).
11. L. F. East and R. P. Hoxey, "Low-speed three-dimensional turbulent boundary layer data. Parts 1, 2," Report and Memo No. 3653, Aeron. Res Council, London (1971).
12. L. G. Loitsyanskii, Laminar Boundary Layer [in Russian], Fizmatgiz, Moscow (1962).
13. L. F. East, "Measurement of the three-dimensional turbulent boundary layer induced on the surface of a slender delta wing by the leading-edge vortex," Report and Memo No. 3768, Aeron. Res Council, London (1975).
14. A. K. Rastorgi and V. Rodi, "Computation of arbitrary three-dimensional turbulent boundary layers," RTK, **16**, No. 2 (1978).
15. T. Sebesi, "Computation of arbitrary boundary layers. II. Three-dimensional flows in Cartesian coordinates," RTK, **13**, No. 8 (1975).
16. J. A. Fillo and R. Burbank, "Computation of arbitrary three-dimensional laminar boundary layers," RTK, **10**, No. 3 (1972).
17. L. M. Vetlutskaya and V. N. Vetlutskii," Laminar boundary layer on a plate with an obstacle," ChMMSS, **10**, No. 3 (1979).